Proposal for Drell-Yan Measurements of Nucleon and Nuclear Structure with the FNAL Main Injector.

The P906 Collaboration

April 9, 1999

Abstract

We propose to make precise measurements of the fractional momentum (x) dependence of the ratio of the d-antiquark to u-antiquark distributions in the proton, $\bar{d}/\bar{u}$, using proton induced Drell-Yan reactions at 120 GeV. Recent E866 measurements unexpectedly suggest considerable x dependence in this ratio at x >0.2. High intensity primary proton beams from the Main Injector make it possible to extend the x range of the E866 measurements with high precision. The apparatus will also be used to precisely measure the change in the $\bar{u}$ distributions in nuclear targets at x >0.2.

Contents

P906 Collaboration

L. D. Isenhower, M. E. Sadler, R. S. Towell
Abilene Christian University, Abilene, TX 79699

D. De Schepper, D. F. Geesaman (Spokesman), B. A. Mueller,
T. G. O'Neill, D. H. Potterveld
Argonne National Laboratory, Argonne IL 60439

C. N. Brown
Fermi National Accelerator Laboratory, Batavia, IL 60510

G. T. Garvey, M. J. Leitch, P. L. McGaughey, J.-C. Peng, P. E. Reimer
Los Alamos National Laboratory, Los Alamos, NM 87545

R. Gilman, C. Glashausser, X. Jiang, R. Ransome, S. Strauch
Rutgers University, Rutgers, NJ 08544

C. A. Gagliardi, R. E. Tribble, M. A. Vasiliev
Texas A & M University,College Station, TX 77843-3366

D. D. Koetke
Valparaiso University, Valparaiso, IN 46383

1 Introduction

While proton structure functions have been measured in deep inelastic scattering over ranges of five-orders-of-magnitude in both the fractional momentum of the parton, x, and the virtuality of the incident photon, Q^2, the factorizable, non-perturbative parton distributions must be determined by phenomenological fits e.g. [1, 2, 3, 4]. Each time new data have tested underlying assumptions of the phenomenology that were unconstrained by known symmetries, the phenomenology has been found wanting. For example, no known symmetry requires the equality of the $\bar{d}$ and $\bar{u}$ distributions in the proton, but, until 1991, this was a common assumption. Following the NMC observation [5] that the integral of $\bar{d} - \bar{u}$ is non-zero, NA51 [6] used the Drell-Yan process to confirm this difference and E866 [7, 8] recently measured the x dependence of $\bar{d}/\bar{u}$ and $\bar{d} - \bar{u}$ from $0.03 < x < 0.32$. The E866 results for $\bar{d}/\bar{u}$ are shown in Figure 1 along with the NA51 result and the various parton distribution fits illustrate the impact of inclusion of the E866 data.

Fundamentally, the nucleon structure functions are non-perturbative manifestations of Quantum Chromodynamics. While perturbative QCD quantitatively describes the Q^2 evolution of the parton distributions, the parton distributions themselves have not proved amenable to QCD treatment, although many *models* exist in the literature. Measurements of those distributions that are poorly determined provide vital information on nucleon structure which is used to constrain and refine the phenomenology. For example, in the MRST [4] and CTEQ5 [2] global fits incorporating the E866 results, both the sea and valence distributions differ substantially from previous parameterizations.

We propose to make precise measurements of proton-induced Drell-Yan cross sections on hydrogen and deuterium. These measurements will determine $\bar{d}_p/\bar{u}_p$ for $0.1 < x < 0.45$. The measurements on deuterium are also directly sensitive to $\bar{d}_p + \bar{u}_p$ over this same range. We also propose to measure proton-induced Drell-Yan cross sections on nuclear targets. Our present knowledge of the flavor dependence of the nuclear parton distributions limits the understanding of the nuclear dependences that have been observed. (e.g. [9]). These nuclear measurements also provide a direct comparison with neutrino data on nuclear targets which are currently used to measure $\bar{d} + \bar{u}$. Our results could have implications in other areas. For example, in proton-proton collider experiments the highest energy scales are achieved via $q\bar{q}$ annihilation of large x partons. The ratio of $\bar{d}/\bar{u}$ results from a competition between non-perturbative and QCD gluon splitting contributions and high x results may provide constraints on the gluon distributions at high x which evolve into the antiquark distributions needed at high mass scales.

2 Physics Discussion

To lowest order, the Drell-Yan process, virtual photon production in hadron-hadron collisions, depends on the product of quark and antiquark distributions in the beam and target as:

$$\frac{d\sigma}{dx_1 dx_2} = \frac{4\pi\alpha^2}{9sx_1x_2} \sum_i e_i^2 (q_i^b(x_1, Q^2)\bar{q}_i^t(x_2, Q^2) + \bar{q}_i^b(x_1, Q^2)q_i^t(x_2, Q^2)) \qquad (1)$$

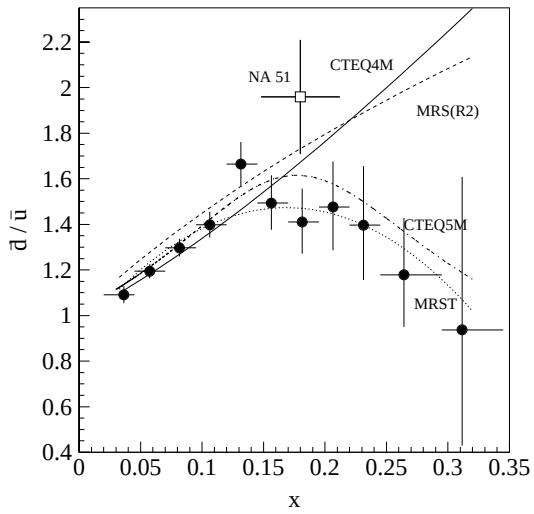

Figure 1: FNAL E866 results[7] for the x dependence of the ratio $\bar{d}/\bar{u}$ of the proton at a mass scale of 7.35 GeV. The square is the NA51 result at a mass scale of 5.2 GeV [6]. The solid (dashed) curve represents the CTEQ4M [1] (MRS(R2) [3]) parameterization prior to the E866 results. The dot-dashed (dotted) curve is the CTEQ5 [2] (MRST [4]) parameterization which included the E866 data in the fitting procedure.

where the superscripts b(t) label the beam(target) and the sum is over all quark flavors (u, d, s, c, b, t). x_1 is the fraction of the longitudinal momentum of the beam carried by the quark from the beam and x_2 is the fraction of the longitudinal momentum of the target carried by the quark from the target. The squared total energy of the beam-target system is $s = 2m_t * E_{beam} + m_b^2 + m_t^2$ with E_{beam} the energy of the beam hadron and m_b and m_t the rest masses of the beam and target hadron respectively. In the case of nuclear targets, we will assume the reaction takes place on a component nucleon, $m_t = M_n$, where M_n is the nucleon mass, and the momentum fraction is A (the number of nucleons) times the fraction of the momentum of the quark compared to the entire nucleus. The convention that c=1 is used throughout the text.

The kinematics of the virtual photon—longitudinal center of mass momentum $p_{||}^{\gamma}$, transverse momentum p_T^{γ} and mass M_{γ}—are determined by measuring the two-muon decay of the virtual photon. These quantities determine the momentum fractions of the two quarks:

$$x_F = p_{||}^{\gamma}/p_{||}^{\gamma,max} = x_1 - x_2 \tag{2}$$

$$x_1 x_2 s = M_{\gamma}^2 \tag{3}$$

where $p_{||}^{\gamma}$ is the virtual photon center of mass longitudinal momentum and $p_{||}^{\gamma,max}$ is the kinematic maximum value it can have.

The kinematics are chosen to gain sensitivity to the antiquark distribution of the target with $x_F > 0$ and x_1 large so that the valence quarks of the beam dominate. In this limit the contribution from the second term in eq. (1) is small and with a proton beam the first term is dominated by the $u(x_1)$ distribution of the proton. Under these circumstances, the ratio of the cross sections for two different targets, X and Y, which

have A_X and A_Y nucleons is approximately the ratio of the $\bar{u}$ distributions:

$$\frac{\frac{1}{A_X}\left(\frac{d\sigma^X}{dx_1 dx_2}\right)}{\frac{1}{A_Y}\left(\frac{d\sigma^Y}{dx_1 dx_2}\right)} \approx \left.\frac{\bar{u}^X(x_2)}{\bar{u}^Y(x_2)}\right|_{x_1 \gg x_2}. \tag{4}$$

In this relation the cross sections are defined per nucleus but the parton distributions are conventionally defined per nucleon.

Equation 4 demonstrates the power of Drell-Yan experiments in determining relative antiquark distributions. We wish to extend the measurements made by E866 to relatively large x_2 where the antiquark distributions are small. Beams from the FNAL Main Injector have two primary advantages compared to previous 800 GeV measurements:

- For fixed x_1 and x_2 the cross section is $\propto 1/E_{beam}$. A Main Injector experiment at 120 GeV will have a factor of $\approx$7 larger cross sections compared to experiments with the 800 GeV Tevatron extracted beam.

- Practical limitations in the acceptable luminosity for these experiments are radiation protection limits and the singles muon rates in the detectors. To the extent that the radiation dose scales as beam power, one can take $\approx$7 times the luminosity for the same beam power at 120 GeV relative to 800 GeV. In E866 at 800 GeV, J/Ψ events from the beam dump were a significant contribution to the muon singles rates. At 120 GeV the total J/Ψ production cross sections fall by an order of magnitude when compared to 800 GeV.

We expect that the combination of these effects will allow a factor of 50 improvement in the statistics at high x_2 compared to E866 and E772.

2.1 $\bar{d}/\bar{u}$ of the proton

E866 and NA51 used measurements of the ratio of the Drell-Yan cross sections on deuterium and hydrogen to determine the ratio of $\bar{d}/\bar{u}$ on the proton by assuming the deuterium cross section is the sum of the proton and neutron cross sections and using charge symmetry to equate $\bar{d}_p$ to $\bar{u}_n$. When the antiquarks in the beam and the strange and heavier antiquarks in the target are ignored:

$$\left.\frac{\sigma^{pd}}{2\sigma^{pp}}\right|_{x_1 >> x_2} \approx \frac{1}{2}\,\frac{(1+\frac{d(x_1)}{4u(x_1)})}{(1+\frac{d(x_1)\bar{d}(x_2)}{4u(x_1)\bar{u}(x_2)})}\left(1+\frac{\bar{d}(x_2)}{\bar{u}(x_2)}\right) \tag{5}$$

While this expression illustrates the sensitivity of the experimental ratio to $\bar{d}/\bar{u}$, the E866 extraction of $\bar{d}/\bar{u}$ was performed using eq. (1) (and checked with a full next-to-leading order calculation) and the CTEQ4M distributions for the valence quark distributions, the sum $\bar{d}+\bar{u}$, and the heavier sea quark distributions. The results showed little variation if MRS(R2) or MRST distributions were used. Figure 2 shows the distribution of $x(\bar{d}-\bar{u})$. The $\bar{d}-\bar{u}$ difference is a pure flavor non-singlet quantity: its integral is Q^2 independent [10] and its Q^2 evolution at leading order does not depend on the gluon distribution of the proton.

In perturbative QCD, differences between the $\bar{d}$ and $\bar{u}$ distributions arise only at second order and are calculated to be very small [11]. The large differences seen in

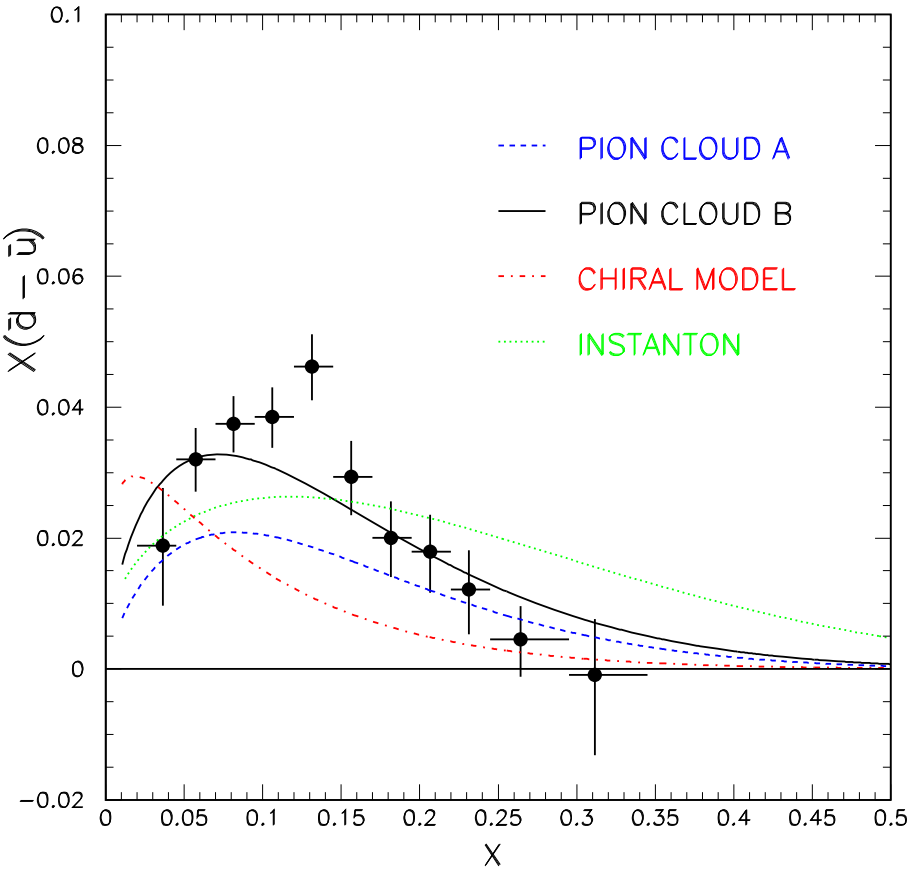

Figure 2: FNAL E866 results[8] for the x dependence of $x(\bar{d}-\bar{u})$ of the proton at a mass scale of 7.35 GeV. The curves represent four model calculations of $x(\bar{d}-\bar{u})$. The solid and dashed curves are the meson-cloud model calculations including nucleons, deltas and pions [8] with differing vertex cut-offs. The dot-dashed curve is a chiral quark model of Szczurek et al. [15] and the dashed curve is the instanton inspired parameterization of Dorokhov and Kochelev [17].

Figures 1 and 2 must be non-perturbative in nature and are likely explained in terms of collective degrees of freedom of QCD at low energy. Early expectations that Pauli blocking would contribute significantly to differences in the light sea were not borne out by calculations [11] (though this point is still debated in the literature [12]). There are three significant approaches which can accommodate large $\bar{d} - \bar{u}$ differences: 1) hadronic models of the meson cloud of the nucleon, 2) chiral quark models which couple mesons directly to constituent quarks and 3) instanton models. Figure 2 illustrates calculations for representative examples of each of these models. An intriguing feature is that in each of these models the flavor and spin distributions of the proton are intimately linked.

The pion cloud model has a tantalizing simplicity and does explain basic features of the data. A proton wave function containing sizable virtual $|n\pi^+\rangle$ Fock states will have an excess of $\bar{d}$ from the valence quarks in the π^+. If one treats the NNπ vertex function as a free parameter one can characterize the experimental distribution to x ≈ 0.2 with "not-unreasonable" vertex functions (dipole vertex functions with a ≈ 1 GeV cut off). The difficulty in this approach is finding justification to truncate the hadronic expansion [13]. A more realistic inclusion of $\Delta(1232)$ isobars leads to a reduction in the predicted $\bar{d} - \bar{u}$ [14] shown as the dashed curve in Figure 2. Again, however, with reasonable parameter choices for the $N\Delta\pi$ vertex function consistent with $pp \to p\Delta$ data, one obtains an approximate description of the $\bar{d} - \bar{u}$ data (solid curve in Figure 2). The resulting probabilities for the $|N\pi\rangle$ and $|\Delta\pi\rangle$ admixtures lead to a prediction for the difference in total spin carried by the u quarks (Δu) and the d quarks (Δd), $\Delta u - \Delta d = G_A$ of ≈ 1.5 [8], providing part of the reduction from the quark model value of 5/3.

Chiral field theories suggest that the relevant degrees of freedom are constituent quarks, gluons and Goldstone bosons. Processes such as $u \to d\pi^+$ and $d \to u\pi^-$ generate a flavor asymmetry in the sea simply because there are more up than down quarks in the proton. The prediction of $\bar{d} - \bar{u}$ in one of the chiral models [15] is shown as the dot-dashed curve in Figure 2. A general feature of these models is an x dependence which is too soft because the models start with the x distribution of the valence quarks.

Instanton effective Lagrangians imply coupling at the tree level between instantons and the valence quarks which leads to a $\bar{d} - \bar{u}$ difference. This raises the intriguing possibility that Drell-Yan measurements could provide experimental information on these theoretically very useful but seemingly experimentally inaccessible constructs. Within the framework of the t'Hooft SU(2) effective Lagrangian [16] (which is of the form $\bar{u}_R u_L \bar{d}_R d_L + \bar{u}_L u_R \bar{d}_L d_R$ where the subscripts R and L label the quark helicity) the u quarks generate a $\bar{d}d$ sea and the helicity of the valence quarks is screened [17]. (A flavor SU(3) Lagrangian would also generate $s\bar{s}$ pairs.) Dorokhov and Kochelev fit the NMC measurement of the $\bar{d} - \bar{u}$ integral to a form parameterized to have the expected asymptotes which is shown as the dashed curve on Figure 2. The difference $\bar{d} - \bar{u}$ does not show the p_t dependence expected in ref. [17]. One set of predictions is the relations between the instanton contributions (subscript I in eq. (6)) of the spin and flavor matrix elements, for example:

$$\bar{d}_I(x) - \bar{u}_I(x) = \frac{3}{5}(\Delta u_I(x) - \Delta d_I(x)) \tag{6}$$

It is interesting to note that while this approach gives a reduction in the total spin carried by the quarks in the nucleon, it implies an increase in $\Delta u_I(x) - \Delta d_I(x)$ while in the other

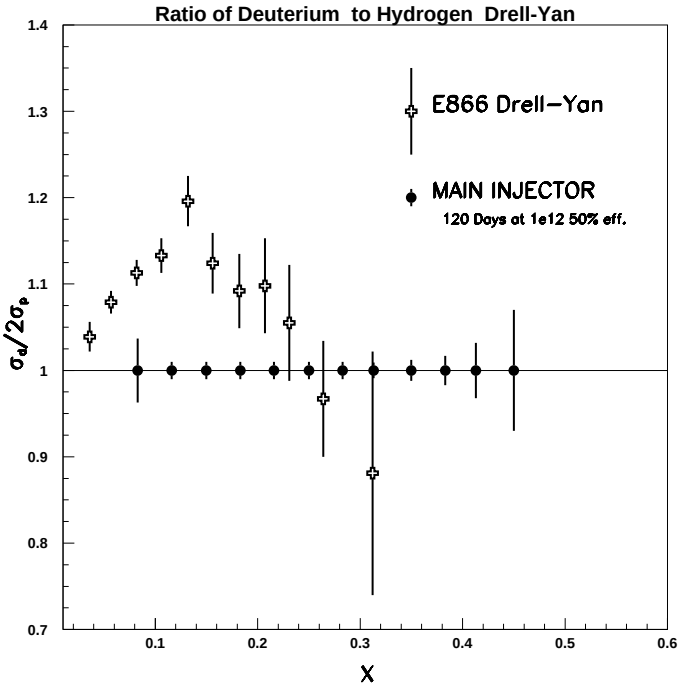

Figure 3: FNAL E866 results[7] for the x dependence of the ratio of $\sigma_d/2\sigma_p$. The statistical uncertainties expected for the measurement proposed here are shown as the error bars on the solid circles (which are arbitrarily plotted at 1.0). The systematic errors are estimated to be less than 1%.

models an increase in the flavor asymmetry causes a decrease in $\Delta u(x) - \Delta d(x)$.

None of these models consistently incorporate the flavor symmetric sea and consequently all substantially overpredict the ratio of $\bar{d}/\bar{u}$ for x >0.23. Unfortunately the error bars on the E866 data become large in this region, due entirely to limited statistics. The pion models tend to level off at a predicted ratio $\bar{d}/\bar{u} \approx 1.5 - 5$ (depending on the baryons and mesons included in the calculations) until $x > 0.5$ where the ratio begins to decrease slowly to unity. The instanton model predicts a ratio of $\bar{d}/\bar{u} \approx 4$ at high x. One possible interpretation of the E886 results is the perturbative gluon mechanism begins to reestablish its dominance over the non-perturbative mechanisms at a lower x value than previously expected. Note that the gluon distribution at high x changed considerably from reference [3] to [4] with a change in the treatment of the fixed target prompt photon data.

The expected statistical precision with which one can measure the ratio $\frac{\sigma^{pd}}{2\sigma^{pp}}$ in an experiment at the Main Injector is shown by the error bars on the solid points in Figure 3 along with the E866 high mass results. E866 has considerably more data at spectrometer settings which emphasize lower masses, and consequently lower x_2, but this represents essentially the complete data set for large x_2. It is apparent that a high luminosity Main Injector experiment can extend the x range of our knowledge of $\bar{d}/\bar{u}$ up to $x \approx 0.45$.

The cross sections on deuterium determine the flavor singlet quantity $\bar{u}_p + \bar{d}_p$ and the extended kinematic range compared to previous measurements will be important in

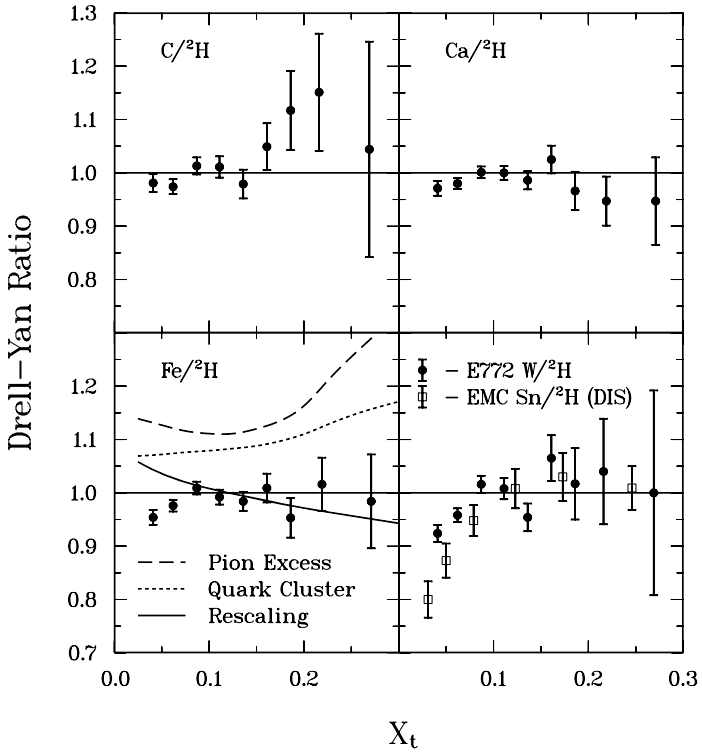

Figure 4: E772 measurements of the ratio of Drell-Yan cross sections on nuclear targets to deuterium [18].

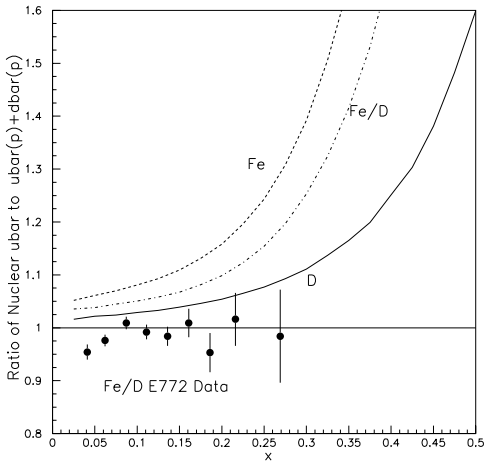

Figure 5: Ratio of $\bar{u}$ in deuterium to $(\bar{u}_p + \bar{d}_p)/2$ (solid) as calculated by Coester [19] including both nuclear motion and pion contributions. The dashed curve is the same quantity for Fe, and the dot-dashed curve is the ratio of iron to deuterium which should be directly comparable to the E772 data [18].

the global fits to determine this quantity with minimal nuclear corrections. As present, neutrino data on nuclear targets place the dominant constraints on $\bar{u}+\bar{d}$. The comparison of the nuclear dependences will be discussed in the next section.

2.2 $\bar{u}$ of Nuclei compared to $\bar{u}$ of deuterium

In the context of nuclear convolution models, virtual pion contributions to nuclear structure functions were expected to lead to sizable increases in sea distributions of the nuclei compared to deuterium. This expectation was shattered by the convincing E772 Drell-Yan measurements [18] (See Figure 4) which showed little A dependence except in the shadowing region. High precision measurements at x larger than E772 could access would provide extremely valuable new information on the nuclear dependence of parton distributions. For the first time, we would have the sensitivity to see the reduction in the nuclear sea distributions predicted in the Q^2 rescaling models. A large rise in the nuclear ratio would provide an important alert that nuclear effects may be important in the deuterium to hydrogen ratio. Figure 5 shows convolution model calculations by Coester[19] of the ratio of $\bar{u}$ in iron and deuterium to $(\bar{u} + \bar{d})/2$ of the proton and the ratio of $\bar{u}_{Fe}/\bar{u}_D$. One can observe that even in this model the predicted nuclear effects in the deuterium-to-hydrogen ratio are small for $x < 0.3$ as compared to the large effects seen in Figure 1. Since this model implies much larger nuclear effects in iron than are compatible with the E772 results, it appears to substantially overestimate the nuclear dependence. By taking comparable nuclear data, we will be able to constrain the possible nuclear effects on the $\bar{d}_p - \bar{u}_p$ measurements and be able to make direct comparisons with antiquark distributions obtained from neutrino data on nuclear targets. Figure 6 illustrates a comparison of the deep inelastic and Drell-Yan results on the ratios of calcium to deuterium along with the expected errors from the measurements proposed here.

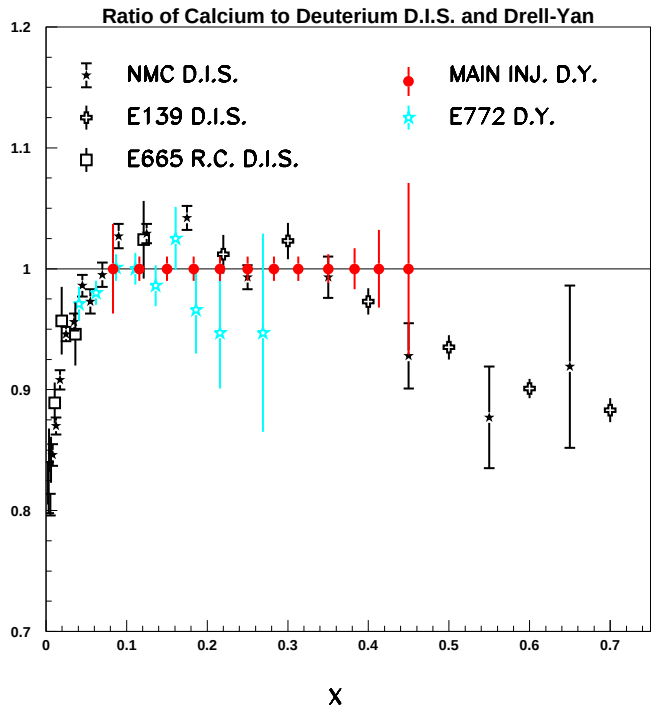

Figure 6: Compilation of deep inelastic and Drell-Yan results on the ratio of cross sections on calcium to deuterium. The statistical uncertainties expected for the measurement proposed are shown as the error bars on the solid circles (which are arbitrarily plotted at 1.0). The systematic error is expected to be less than 1%.

Another nuclear effect that is now of considerable interest primarily in discussions of relativistic heavy ion collisions is the energy loss of partons while passing through cold nuclei. The dominant contribution is believed to be the gluon equivalent of bremsstrahlung. Several different attempts [20, 21, 22] have been made to predict the average energy loss expected for proton-induced Drell-Yan scattering. Data from E772 at 800 GeV/c were used by Gavin and Milana [20] to estimate the initial state energy loss. They ignored shadowing effects and found a surprisingly large result. Further work suggested that the energy loss should be substantially smaller [21]. A detailed analysis has been carried out more recently [22], which suggests that the initial state energy loss should scale as $A^{2/3}$. Drell-Yan data taken for protons on Be, Fe and W during E866 show clear evidence for shadowing and are consistent with the small energy loss estimates. In fact, the results also appear consistent with no measurable energy loss in the initial state. The effect of energy loss as partons pass through nuclei is far from clear. Changing the kinematics by lowering s significantly may help us to understand this process. In particular, the energy loss forms derived in [21, 22] contain a factor of $1/s$, while the energy loss form in [20] is independent of s. Thus, similar measurements of Drell-Yan production on nuclei at the Main Injector will provide important additional information about this question of initial state energy loss and factorization in Drell-Yan processes on nuclear targets (see below).

2.3 Interpretability of the Results

The interpretability of Drell-Yan results as direct measures of the parton distributions is based on the QCD factorization theorems [23, 24]. Bodwin, Brodsky and Lepage [24] give the condition for the minimum beam momentum P_{min} below which initial state QCD interactions become important as:

$$P_{min} \approx \frac{p_\perp A^{2/3}}{x_1} \tag{7}$$

A conservative estimate of $\langle p_\perp^2 \rangle \approx 0.4$ GeV^2 (Ref. [24] uses 0.25 GeV^2) yields a typical transverse hadronic scale $p_\perp$ on the order of 0.6 GeV and a minimum beam momentum of 23 GeV for $x_1 > 0.3$ and a calcium target, comfortably below the 120 GeV considered here.

2.4 Possible Future Measurements

This proposal focuses on measurements with the primary proton beam. A number of other interesting measurements could be made with this spectrometer. We have previously submitted a letter of intent for Drell-Yan measurements with polarized protons on a polarized proton target to determine the spin structure of the sea distributions. When a polarized proton beam becomes available from the Main Injector, the present apparatus would be immediately suitable for that experiment. Even with an unpolarized beam there appear to be interesting correlations one can measure with Drell-Yan on a polarized proton target [25]. Intense secondary meson beams would open up new possibilities such as a more accurate determination of the charged kaon valence parton distributions or measurements of the ratio of d/u distributions of the proton as $x \to 1$.

3 Experimental Apparatus

The experimental apparatus leans heavily on the E605, E772, E789 and E866 experience for the best technique to handle high luminosities in fixed target Drell-Yan experiments. The key features of the apparatus are:

- Relatively short (<15% interaction length, L_I) targets to minimize secondary reactions in the target.
- Two independent magnetic field volumes, one to focus the high transverse momentum muons and defocus low transverse momentum muons and one to measure the muon momenta.
- A 15 L_I hadron absorber to remove high transverse momentum hadrons.
- A 30 L_I beam dump at the entrance of the first magnet.
- Zinc and concrete walls for muon identification at the rear of the apparatus.
- Maximize the use of existing equipment consistent with the physics goals.

As will be discussed below, the apparatus can be almost completely constructed by reusing or refabricating existing equipment. Only the first magnet requires a significant construction effort.

The lower beam energy has two disadvantages relative to 800 GeV experiments.

- The corresponding lower particle energies lead to increased probabilities for muon decay of the produced hadrons. This is partially compensated by reducing the target-to-hadron-absorber distance to 1.3-1.8 m.
- The lower energy muons multiple scatter more easily in the hadron absorber.

We wish to optimize the design for events with large x_2 and $x_F \approx 0.2$. For scale, the muons generated by a 7 GeV virtual photon with $x_F = 0.2$ which decay perpendicular to the direction of motion (in the virtual photon rest frame) will in the laboratory have momenta of 33 GeV, an opening angle of 210 mr and transverse momenta of 3.5 GeV.

A sketch of the apparatus showing trajectories for muons from 90° decays at $0 < x_F < 0.4$ is shown in Figure 7 (bend plane view) for a 7 GeV mass virtual photon. Figure 8 illustrates the non-bend plane view. The coordinate system has Z along the beam axis with z=0 at the upstream face of the first magnet. X is horizontal, (beam West) and Y is vertical, increasing upward, for a right handed coordinate system.

3.1 Beam and Targets

The requirements for the beam are 10^{12} protons per pulse with a maximum beam spot size of 5 mm vertical by 10 mm horizontal and maximum divergence of 2 mr in each direction. The primary beam will stop in a 170" long trapezoidal Cu beam dump starting with a 3" vertical height at z=0 extending to a 12" vertical height at z=170". Since the dump will

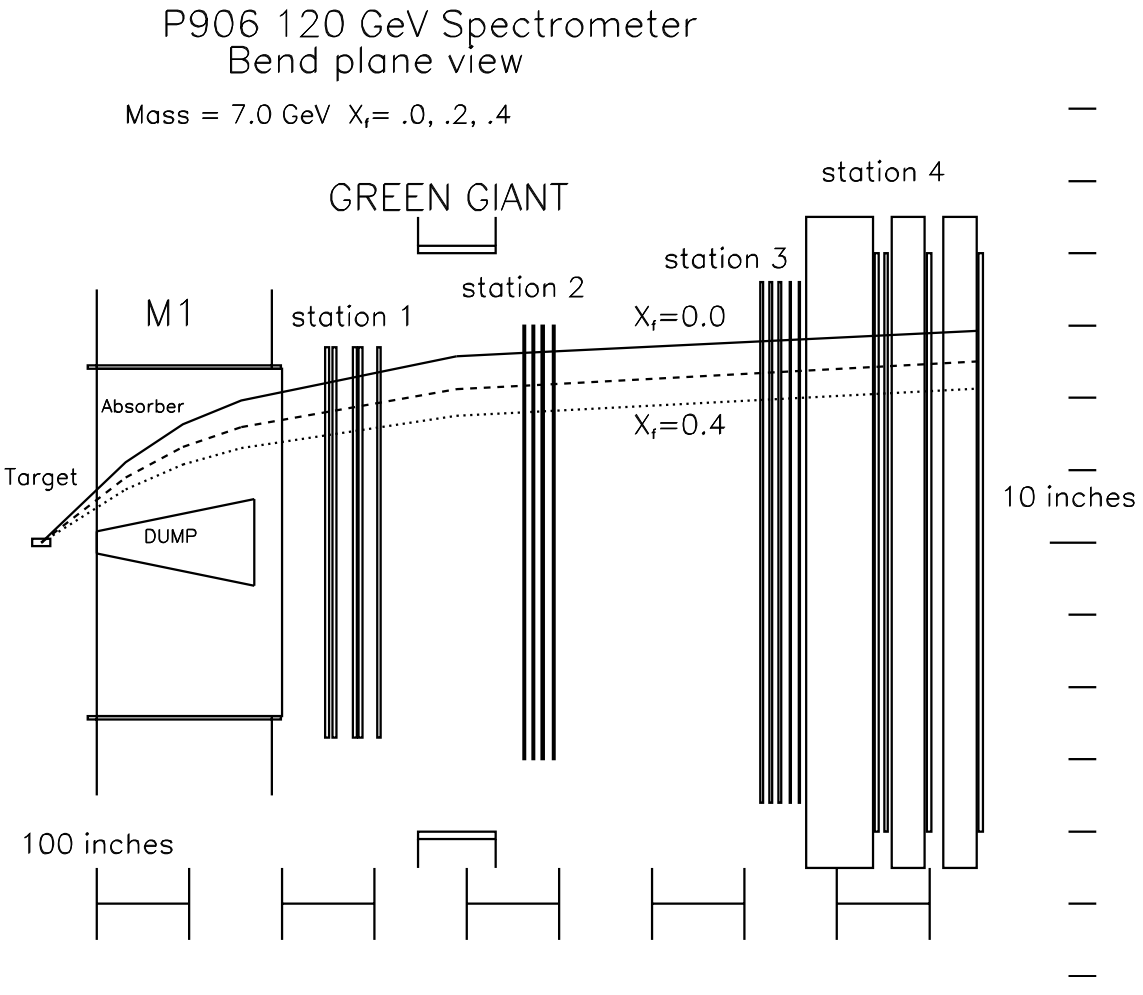

Figure 7: Bend plane view of the trajectories of one of the two muons resulting from the muon decay of a 7 GeV virtual photon (which has x_F of 0.0, 0.2 or 0.4) in an 8 T-m spectrometer.

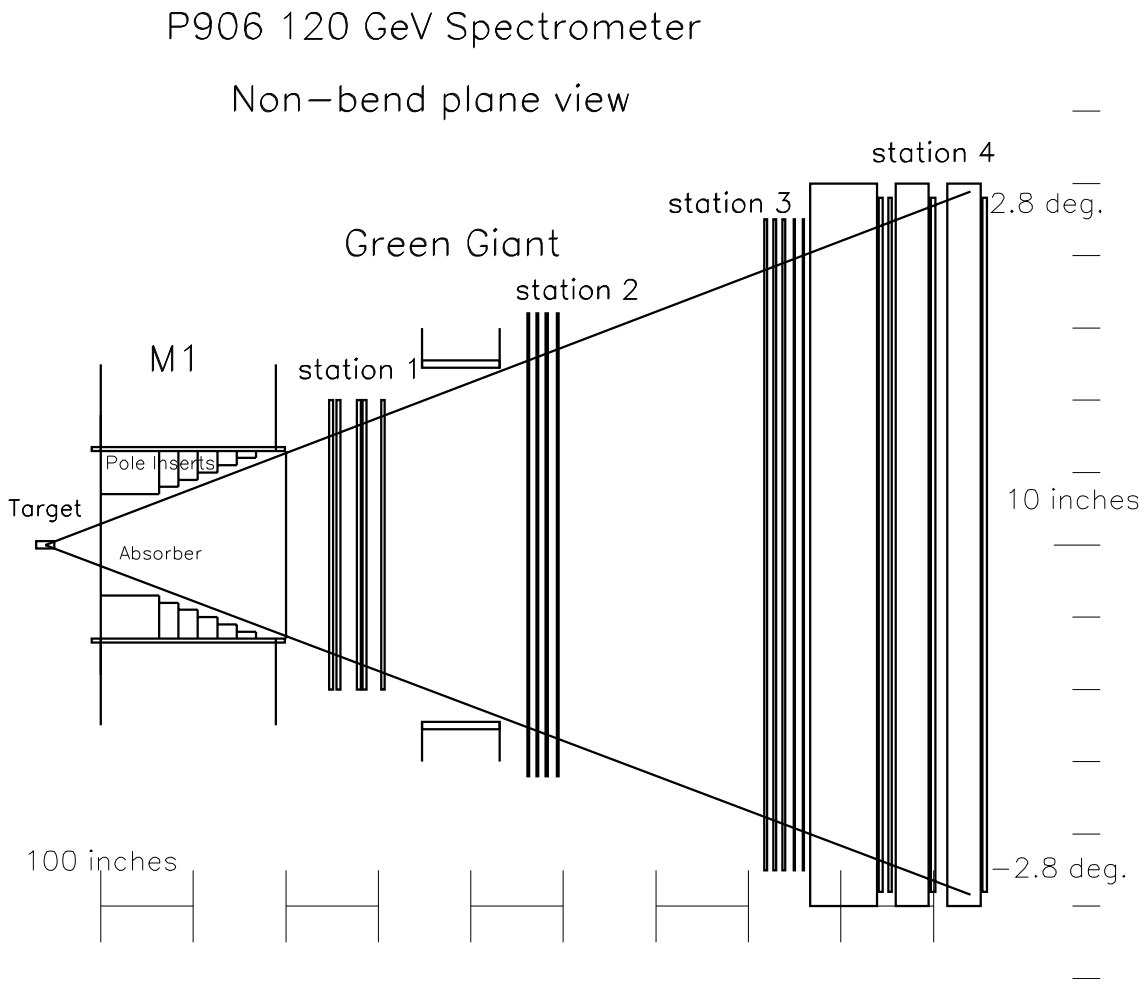

Figure 8: Non-bend plane view in an 8 T-m spectrometer. Only muons which pass around the beam dump in the bend plane contribute to the acceptance and so the beam dump is not shown.

Table 1: M1 Magnet Characteristics

Length	189 in
Width	95 in
Height	198 in
Vertical Aperture	48 in
Horizontal Aperture without inserts	26 in
Field Integral	8.14 T-m
Ampere-Turns	670230
Current	2394 Amp
Power	0.58 Mwatt
Inlet Water Temperature	38 deg C
Temperature Rise	25 deg C
Water Flow	88 gal/min
Weight of Pole Inserts	9.5 t
Weight of Coils	19 t
Weight of Return Yoke	420 t
Total Weight	450 t

absorb an average of 6400 watts of beam power, we anticipate it would be water cooled with a closed loop recirculation system like the E866 dump.

The experiment would use 20" long liquid hydrogen and deuterium targets, three nuclear targets of $\approx$ 10 gm/cm^2 thickness and a dummy liquid target cell. The targets would be remotely interchanged roughly every 30 minutes. The rapid Main Injector spill cycle will require blocking the beam for on the order of 30 sec to allow for target motion. The exact choice of nuclear targets has not been made but they are likely to be carbon, calcium or iron and tungsten. An advantage of iron would be a more direct comparison with the CCFR data. Tungsten would extend the A dependence studies to a heavy nucleus, especially for the energy loss studies.

The end of the target is located only 1.3 m from the beam dump. We anticipate installing a remotely movable Pb curtain between the target and the dump to reduce the radiation impact on target service operations.

3.2 Magnets

The purpose of the first magnet of the spectrometer is to contain the high transverse momentum muons and to bend low momentum muons out of the experimental acceptance. The optimal performance would be obtained with a $\approx$2.5 GeV p_t kick ($\approx$ 8 T-m) large aperture 48" (y) by 26" (x) magnet. Reasonable Drell-Yan acceptance may be retained, provided the aperture of the downstream spectrometer is large enough, for lower field integrals but the singles rates increase dramatically to an unacceptable level. Even with the present design we must be prepared for 100 MHz instantaneous rates in the first set of wire chambers.

An 189" long 8 T-m large aperture magnet can be constructed using 33% of the

Table 2: Jolly Green Characteristics

Length	84 in
Width	135 in
Height	190 in
Vertical Aperture	96 in
Horizontal Aperture	49.14 in
Field Integral	1.65 Tm
Ampere-Turns	1010000
Current	980 Amp
Power	0.89 Mwatt
Inlet Water Temperature	35 deg C
Temperature Rise	22 deg C
Water Flow	152 gal/min
Total Weight	220 t

iron from SM12 in Meson East with new coils, following the same general principles as SM3. The characteristics of this magnet are given in Table I. Iron inserts will provide a tapered horizontal aperture of 98 mr opening angle tailored to the aperture of the second magnet. By using existing iron pieces for the return yoke, there should be minimal need to machine the radioactive iron. With such a magnet, there appear to be no experimental barriers to completing the measurement proposed here. The aperture around the beam dump is filled with a graded hadron absorber consisting of 80" of graphite, followed by 40" of copper then 40" of graphite and 40" of Borated Polyethylene.

The muons will lose ≈ 3.5 GeV in energy passing through the absorber and multiple scatter by an average angle of $\approx 170/p_\mu$ mr. This level of multiple scattering will still permit acceptable virtual photon mass resolution ($\approx$240 MeV) and acceptable vertex resolution to separate target and beam dump events for muon energies greater than 15 GeV. Due to the long target length relative to the target-to-absorber distance, the target position provides minimal additional track constraints for the mass measurement.

The second magnet must provide the accurate momentum determination and have a large acceptance. The existing SM3 magnet would be ideal, but is being moved to C0. The most suitable available FNAL magnet appears to be the Jolly Green Giant (JGG) which is currently in Lab G. At present, the JGG has a turn-to-turn short in one of its coils. We would need to have the short repaired to improve the p_t kick to 0.5 GeV (estimates of the cost of the repair are available). The characteristics of the Jolly Green Giant are given in table 2.

We also expect that for radiation protection purposes, the spectrometer, like the Meson-East spectrometer, will need to be vertically bending. If so the JGG would require modification to accommodate this since it is presently configured as a horizontal bending (vertical field) magnet.

If the Jolly Green Giant or another comparable magnet is not available, a suitable replacement could be constructed following the same techniques and using another 8 pieces of the SM12 return yoke. The coil cost would be roughly half of the cost of the

Table 3: Wire Chamber Specifications and Singles Rates

Station	Type	X size (cm)	Y size (cm)	wire spacing (mm)	wire orientations	Number of Channels	Singles Rates (MHz)
1	MWPC	101.6	137.2	2.0	Y,U,V,Y,Y',U',V'	7000	40
2	DC	137.7	149.9	10.2	Y,Y',U,U',V,V'	1000	10
3	DC	203.0	162.4	20.3	Y,Y',U,U',V,V'	700	2
4	Prop. Tube	254.0	211.0	10.0	Y, Y', X, X'	900	2

new coil for M1. This would effectively be a copy of SM3 but with only half the field integral.

The absorber configuration was optimized based on GEANT simulations. The 40" of copper helps to eliminate particles which meander out of the dump. The instantaneous single rates at each of the detector stations are given in Table 3. The dominant single contribution is muons from the decays of hadrons in the dump.

3.3 Tracking Chambers

The high instantaneous rates at station 1 lead us to plan for rates up to 100 MHz. We propose to use Multi-Wire-Proportional-Chambers with a 2 mm wire spacing. The first three planes would be MWPC's used in E605 with existing electronics. The stereo angles of the U and V wires are $\pm$ 14 degrees. The following four planes would use two existing E871 MWPC's, each covering half the x acceptance arranged with a 4" horizontal gap at x=0. The frames of the two chambers would overlap in this gap. While multiple scattering in the frames does not significantly deteriorate the resolution, this x=0 stripe avoids the highest count rate areas (at the maximum y). The stereo angle of these planes is $\pm$ 26 degrees. Existing E871 preamplifier - discriminator - readout would be used. Each of these wire chambers has 3 rf bucket hit resolution and would run with a fast gas (CF4/isobutane, 80:20). The readout would consist of 7000 channels of coincidence registers. All the electronics and readout currently exist (E871 has 20000 wire chamber channels).

Stations 2 and 3 would use the existing E605/E772/E866 drift chamber stations 2 and 3. They are capable of 250 μm resolution with Ar/Ethane (50:50) gas. The stereo angle is $\pm$ 14 degrees. Existing preamplifiers and discriminators would be adequate. A 1700 channel multi-hit TDC system (LRS 3377 modules are expected to be available from PREP) is required for good efficiency and rate capabilities.

Station 4 would be constructed of limited streamer tubes with a 1 cm pitch operated in proportional mode using existing amplifiers and discriminators from E866. Readout would be identical to the MWPC's and add 900 channels to the electronics and coincidence register total.

We have studied the rate dependence of the pattern recognition efficiency in Monte Carlo simulations to ensure that this choice of chamber configuration is acceptable. With 2.5 times the rates given in Table 3, we find only a 4% decrease in efficiency, on the same

scale with the level of rate dependent effects we were able to deal with in E866.

3.4 Scintillator Hodoscopes

Scintillator hodoscope planes will provide the hit information for the hardware trigger system, just as they have in E866. There will be a total of eight planes, four to measure track y (bend plane) locations and four to measure track x locations. There will be a y hodoscope plane associated with each of the four detector stations – referred to as Y1, Y2, Y3, and Y4. They will contain 32 channels apiece, separated into 16 channels on the right side of the spectrometer ($x < 0$) and 16 channels on the left side ($x > 0$). There will be x hodoscope planes associated with detector stations 1 and 2, plus two additional planes as part of station 4 – referred to as X1, X2, X4A, and X4B. They will contain 32 channels apiece, separated into 16 channels for the lower half of the spectrometer ($y < 0$) and 16 channels for the upper half ($y > 0$). This segmentation will provide a logical division of each hodoscope plane into quadrants, allowing the trigger system to place tighter geometric constraints on the tracks than was done during E866.

All of the scintillators within a given y hodoscope plane will be the same size. The individual scintillators within hodoscope planes X4A and X4B will all be the same angular size. In contrast, the four X1 and four X2 scintillators closest to $x = 0$ will subtend half the angular range, and the scintillators furthest from $x = 0$ will subtend 1.5 times the angular range of the X4A and X4B scintillators and the remaining X1 and X2 scintillators. This segmentation minimizes the number of hodoscope channels in stations 1 and 2 that may be in coincidence with given channels in X4A and X4B, after accounting for the multiple scattering of the muons through the various absorbers in the spectrometer.

While many of the hodoscopes could be fabricated primarily by recutting and polishing the existing E866 scintillators to the sizes required for the new spectrometer, we believe it is safer, given their age, to plan on constructing new scintillators and light guides for this experiment. We propose to reuse the phototubes and bases from the existing E866 spectrometer and purchase 60 new phototubes and bases for the additional channels. The existing E866 high voltage distribution systems will suffice to power the eight hodoscope planes.

During E866, the anode signals from each phototube were sent to LeCroy 4416 leading-edge discriminators. The discriminator outputs were reshaped by custom synchronizer/stretcher modules to provide clean, single RF bucket time resolution for all hodoscope planes except station 4, which had slightly worse than single bucket resolution. The higher background rates anticipated at the Main Injector due to the increased beam current make it very important to achieve clean, single RF bucket time resolution for all hodoscope planes. Given past experience, this should be straightforward with the existing discriminators for the hodoscopes in stations 1 and 2, and for the X4A and X4B planes. The longest scintillators in the spectrometer, those for Y4, will be only 7" shorter than the station 4 scintillators during E866 and we propose to use phototubes on each end of these scintillators and 32 channels of mean timers to provide single bucket resolution. We already have enough synchronizer/stretcher modules in hand to instrument the entire new spectrometer.

3.5 Muon Identification

Final muon identification is provided with a absorber wall, 81 cm of concrete followed by 92 cm of zinc and 10 cm of Pb, followed by 2 planes of streamer tubes and the X4A scintillators, then 92 cm of concrete followed by the Y4 and X4B scintillators and finally 92 cm of concrete followed by 2 planes of streamer tubes. The present E866 muon identification walls provide enough material for the smaller P906 wall [26].

3.6 Trigger

The hardware trigger system will examine the scintillator hodoscope hits to identify patterns characteristic of high mass muon pairs produced in the target. It will be conceptually similar to the system that was developed for E866 [27]. However, it will be enhanced substantially compared to the previous system, primarily to improve its ability to reject random coincidences that appear to form a candidate high p_t muon track. Such random coincidences represented over half of the apparent muon tracks observed during the E866 intermediate mass $\bar{d}/\bar{u}$ running, and the background rates in the spectrometer due to soft muons are expected to be even higher at the Main Injector. The trigger modifications will also permit us to implement two-dimensional masking of wire chamber hits during event analysis, based on the active hodoscope roads, which will reduce the combinatorics in the wire chamber track finding. Notably, this will minimize the frequency of hit- and track-bank overflows, one of the sources of rate-dependent reconstruction inefficiency that we encountered during E866. Finally, the trigger modifications will permit us to replace a number of custom CAMAC modules from the E866 trigger system that are now nearly 20 years old with new, more reliable and flexible, commercial units.

Electronically, the hardware trigger will consist of a single decision stage, implemented as a three-step parallel pipeline. In the first step, the outputs from the hodoscope synchronizer/stretcher modules will be routed to a set of LeCroy 2367 Logic Modules. Eight modules will be dedicated to identifying four-fold Y1-Y2-Y3-Y4 coincidences characteristic of high p_t single muons produced in the target. Each time they observe a candidate track, they will output a bit indicating its charge, the side of the spectrometer (left or right) where it is located, the quadrant the track passed through at Y1, and the actual y location of the track at Y4. In general, Y1-Y2-Y4 triple coincidences would suffice since the spectrometer analyzing magnet is located between stations 1 and 2, and that is in fact how candidate tracks were identified during E866. Adding the extra constraint that the appropriate channel of Y3 must have a hit will help reject apparent tracks that actually consist of a random coincidence between hits in stations 1 and 2 due to one muon and a hit in station 4 due to another.

The $\bar{d}/\bar{u}$ experiment will only be interested in a limited number of potential track roads through the spectrometer. However, the eight LeCroy 2367 modules required to identify all of those tracks contain enough additional internal logic and I/O capability to cover the entire phase space of four-fold Y1-Y2-Y3-Y4 coincidences associated with real tracks originating from either the target or the beam dump. This will provide maximal flexibility when designing triggers for study purposes or ancillary measurements.

Four additional LeCroy 2367 modules will be dedicated to identifying candidate tracks originating from the target that include coincidences among at least three of the four

planes X1-X2-X4A-X4B. Each time they observe a candidate track, they will output a bit indicating the side of the spectrometer where it is located, the quadrant the track passed through at X1 and X2, and the actual x location of the track at X4A and X4B. This represents a significant upgrading of the tracking capability of the hardware trigger in the x direction, compared to E866, and will permit us to provide full two-dimensional constraints on the tracks. It will also make continuous monitoring of the efficiency of the y hodoscopes practical. This may prove to be important because our ability to average over long-term variations in the spectrometer efficiency between targets will be reduced at the Main Injector, since we will be unable to change amongst the various targets as frequently as we did during E866. In contrast, for E866 special hodoscope efficiency studies were run every few weeks. They consisted of a series of runs utilizing a special trigger configuration, sequentially turning off the high voltage on sets of x hodoscopes near the center of the spectrometer.

The second step in the trigger pipeline will combine the x and y tracking results from the first step to identify events with candidate high p_t muons present. This will be done in a pair of LeCroy 2367 modules, one dedicated to tracks on the left side of the spectrometer and one dedicated to tracks on the right side. The candidate muons will be characterized according to their charge, the side of the spectrometer on which they are located, and a rough measure of their p_t. Events will also be tagged that appear to have two muons with opposite charges present on the same side of the spectrometer.

In parallel with the first two steps of the main trigger sequence, OR's of all the scintillators on each side of each plane will be generated and routed to a Track Correlator [27] to generate simple cosmic ray and noise triggers for diagnostic purposes. This same procedure was utilized during E866, and the same CAMAC and NIM electronics will be reused at the Main Injector.

The final step in the trigger pipeline will generate the actual triggers, handle the experiment busy logic, and strobe the read-out electronics. This step will either be performed with one additional LeCroy 2367 module or with the Track Correlators and Master Trigger OR that were designed and constructed for the E866 hardware trigger [27]. The primary physics trigger will consist of a coincidence between two candidate $x-y$ tracks of opposite charges, on either the same or opposite sides of the spectrometer. If we find that the background trigger rate due to low mass muon pairs is higher than desirable, we will combine the rough measures of the p_t for the two muons from the previous step to provide a crude effective mass cut on the muon pair in hardware. A similar procedure, but with less granularity than we anticipate with the new trigger system, was adopted for several of the data sets taken during E866. For example, it reduced the raw trigger rate during the E866 intermediate mass $\bar{d}/\bar{u}$ data taking by a factor of three, with essentially no reduction in efficiency for the Drell-Yan muon pairs of interest. Two triggers will be used to determine the rate of random coincidences between two muon tracks in the same RF bucket, both of which originate from the target and, thus, are indistinguishable from a real Drell-Yan muon pair. One of these triggers will record events that contain two muons of the same charge when they are located on opposite sides of the spectrometer, while the other will record a prescaled set of single-muon events. E866 has demonstrated that we can obtain an excellent simulation of the random coincidence background by combining muons from single-muon triggers into pairs, then normalizing their number to the observed rate of like-sign coincidences. Two additional triggers will select prescaled

samples of events that contain a candidate track in either the x or y direction, but not necessarily both. The events with x tracks will be used to monitor the absolute efficiencies of the y hodoscopes, and the events with y tracks will be used to monitor the absolute efficiencies of the x hodoscopes. The last trigger will provide a luminosity-weighted read-out of all detector elements during random RF buckets, independent of the status of any of the spectrometer hodoscopes. This will be used to provide an unbiased measure of the background occupancy rates throughout the spectrometer, which are very important for estimating rate-dependent reconstruction inefficiencies.

3.7 Discussion of Rates

Rates have been estimated using two different Monte Carlo codes. The primary one is a modified version of the "Fast Monte Carlo" that was written many years ago to estimate acceptances in E605/E772/E789/E866. For P906, the code has been modified to make the spectrometer configuration more flexible and to include additional sources of muons. This Monte Carlo simulates muons from Drell-Yan, resonance production (J/ψ, ψ', Υ, Υ', Υ''), and π, K and charmed meson decays. It can track single muons or pairs through the entire spectrometer in order to estimate signal and background rates with realistic hardware trigger simulation. It also simulates the traceback of the muon tracks to the target so that realistic tracking cuts may be imposed and the ultimate resolutions of the spectrometer can be estimated. The second code is a modified version of a GEANT-based Monte Carlo that was originally written to optimize the design of the hadron absorber wall in E866. Unlike the first code, this Monte Carlo only tracks particles as far as Station 1. However, it tracks all particle types, rather than just muons, so it is more useful for configuring the hadron absorber that will fill the aperture of the large M1 magnet. Both codes have been demonstrated to give a reasonable description of the rates that were observed during E866, and they give consistent results for the flux of muons with momenta above 3 GeV/c that should be present in Station 1 at the Main Injector.

The physics trigger rate for the experiment is expected to be 0.95 Drell-Yan events per spill for 10^{12} protons incident on the liquid hydrogen target and twice that for the liquid deuterium target. Approximately 1/3 of the Drell-Yan events will pass tracking cuts to eliminate events from the dump and a minimum mass cut of 4.2 GeV to eliminate ψ' events. In total, we expect about 70 real pairs per spill to pass the trigger, with most of them being J/ψ events produced in the beam dump.

In addition to the real pairs, there will be a significant number of triggers from random coincidences of two independent muon tracks. When running with the liquid hydrogen target, the primary source of background single muons will be π and K decay-in-flight in the beam dump. When running with the liquid deuterium target, the decay-in-flight backgrounds from the target and the beam dump will be nearly the same. We estimate that there will be less than 160 random coincidence triggers per spill with the liquid hydrogen target and less than 270 random coincidences per spill with the liquid deuterium target, including both opposite-sign pairs and like-sign pairs. These numbers are based on the assumption that, in addition to the single-muon tracks that the fast Monte Carlo predicts should pass the trigger, we will have an extra $\approx$30% random contribution to the single-muon hardware trigger yield. This fraction is somewhat less than was present in

E866 since the new trigger system will be more selective. These random trigger rates do not include the additional suppression that we will obtain by constraining the apparent mass of the pair in hardware.

We will also take approximately 80 study triggers per spill – including prescaled single muons to study the random background, triggers to monitor the efficiency of the hodoscopes, and triggers to investigate any rate-dependence that may be present in the data analysis. Therefore, overall we expect approximately 310 triggers per spill on the liquid hydrogen target and 420 triggers per spill on the liquid deuterium target. Meanwhile, the trigger rates for the nuclear targets will be between these two. We will assume a trigger rate of 1kHz for planning purposes. With full analysis cuts, the real to random rate is expected to be better than 2 to 1 at all x_2 values, and much better than that at large x_2.

3.8 Data Acquisition System

In order to achieve the goals put forward in this proposal, the data acquisition system must be able to: (1) digitize and move to tape detector hits from MWPC's, hodoscopes, streamer tubes and drift chambers at trigger rates of up to 1 kHz with very small dead time; (2) include information on the trigger condition in the data stream; (3) provide for on-line monitoring of detector efficiencies and the status of main system components; (4) provide for control of experimental systems such as moving targets and programming trigger modules. All of these capabilities were available in the DAQ system which was used for Fermilab experiment E866. However, several features of the E866 system must be changed to accommodate the MI experiment.

The readout system for E866 used the TRANSPORT interface, which was built by the NEVIS electronics group in 1980, to hoist data from custom built TDC's and coincidence registers to tape. Many problems were encountered with that system during the startup of E866. We also experienced intermittent problems with it during data acquisition. Both the age of the system and the constraints that it imposes on the data stream require that we replace it for the MI experiment. Because they are to operate in a high rate environment, the drift chambers for the MI experiment need to be read out with multi-hit TDC's which precludes using the TDC's from the E866 readout system.

Most of readout requirements for the proposed experiment can be met by the front end system that has been assembled for Fermilab experiment E871. We request that the CR's, FEM's, interface and buffer memory and one VME system used by E871 be moved to this MI project after the last 800 GeV fixed target run is completed and E871 is decommissioned. The E871 system will provide a high speed readout path for the MWPC's, hodoscopes and proportional tubes configured here. We will add multi-hit TDC's, and the appropriate interface connection to the Processor Bus, to read out the drift chambers.

The computer architecture used in E871 is very similar to that planned for this project. Our trigger rates, however, will be much lower than those for E871 and event lengths will be comparable so the dead time using their system should be extremely small. As in E871, data will be moved from front end modules to buffer memory and then written out on DLT units. One DLT should suffice to handle the bandwidth since we anticipate average event lengths of less than 1.5 kbytes and trigger rates less than 1 kHz. Event

sampling will be done to monitor wire chamber and hodoscope efficiencies using UNIX based workstations or PC's running LINUX.

The DAQ system for this project will follow DART standards and use DART software. This represents another break from the E866 system which did not use DART. The E871 DAQ system uses DART so the front end readout is already compliant with DART standards. With the exception of trigger programming, the remaining system requirements for the MI experiment proposed here are already available in DART software packages.

3.9 Analysis

The analysis of the data accumulated in these measurements should be straightforward, both in offline production and for online monitoring. We expect that the analysis will be similar to that done for E866 and would employ farms of LINUX PC's. An estimate of the scope of the analysis task can be made from the expected trigger rate of 1 kHz (1/3 kHz average), estimated event size of 1.5 kbytes, and a compute time per event of 20 ms/evt (on an 180 Mhz HP PA8000) based on analysis of data in E866/NuSea. Scaling with floating point performance to a 400 Mhz Pentium II (a current "commodity" PC) we estimate that approximately five of these Pentium CPU's can analyze our data as fast as we would take it. In the counting house we generally want to be able to fully analyze about 10 to 20% of the data as it is accumulated and this could be accomplished with only one or two of these PC's. Naturally, since the typical CPU power per dollar increases by perhaps a factor of two per year, by the time this experiment would actually run the hardware available would even more easily address these analysis problems.

The typical taping rate is estimated to be about 0.5 Mbytes/sec (easily within the bandwidth of present Digital Linear Tape (DLT) technology) and would result in about 43 Gbytes of data on tape per day, or about 5 Terabytes for the entire run. To analyze these data as fast as they were taken means the networks that support distribution of the data would need to transport in excess of 0.5 Mbytes/sec, easily within the capability of 100 base-T networks.

Since the planned detector system would be conceptually similar to that used in E866, the analysis algorithms from E866 should be applicable to the new experiment. Therefore we anticipate reusing much of the old code. Since much of the raw data format will probably be new the data unpacking parts of the code would probably be rewritten in C or C++, while other parts that need not change may remain in Fortran. We also would replace the present CMZ code manager with CVS for code maintenance and cpp for conditional compilation. Tools that we have already used for the PHENIX project at RHIC should aid in this conversion. Since our code already runs on the Fermilab UNIX farms using the Fermilab parallel processing environment (CPS), it should be straightforward to preserve that capability. CPS is already ported and being used on LINUX PC farms at Fermilab.

3.10 Yields

Figure 9 shows the results from a Monte Carlo simulation of the expected yields of this spectrometer for a hydrogen target in 90 days at 50% efficiency running. With an 9

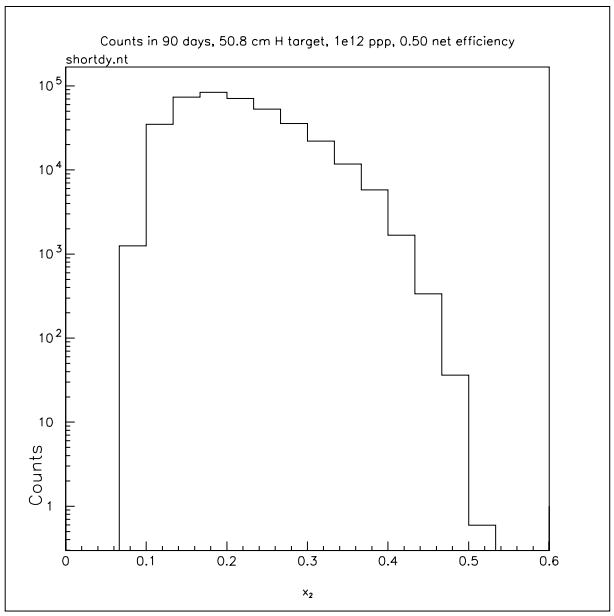

Figure 9: Monte-Carlo results for yields from a 90 day 50% efficiency run with 10^{12} protons per pulse on a 20" long liquid hydrogen target with the apparatus shown in Figures 7-8. This represents all accepted events with masses between 4.2 and 8.5 GeV with $x_F > -.1$. The number of counts will be the same on the nuclear targets and 70% greater on deuterium.

month run at 50% total efficiency (66% accelerator, 75% experiment), we would achieve these yields on 5 targets (hydrogen, deuterium and three nuclear targets, relative running time: 35% H, 26% D, 35% nuclear, 4% Dummy liquid cell) and achieve the relative errors on the ratio of the deuterium to hydrogen cross sections for $x_F > -.1$ shown in Figure 3. E866 was able to maintain systematic errors on the cross section ratio to 1.1%. We also anticipate being able to achieve 1% systematic errors in the ratio.

With these yields, the statistical precision of the extraction of $\bar{d}/\bar{u}$ is shown in Figure 10 relative to the expectation with MRST parton distributions.

4 Costs and Schedule

The source and operating responsibility of each component of the apparatus is given in Table 4. We are searching for additional collaborators to lead the DAQ and DC1 efforts. The expertise for these exists within the collaboration and the equipment in E871 and E866 exists but we have not yet identified the lead groups. Our specific list of requests for FNAL is separated out in the next section. We have assumed that all the existing equipment from E866 is available for this experiment. We have begun discussions with E871 personnel (Kam-biu Luk of UC-Berkeley about the wire chambers and wire chamber electronics, Ping-Kun Teng and Yen-Chu Chen of Inst. of Phys., Academia Sinica about the readout system) about the use of the E871 equipment.

The critical path of the time-line is clearly the construction of the M1 magnet. A preliminary cost estimate is \$900k for the coil and \$220k for assembly [28]. Following

Table 4: P906 Apparatus Responsibilities

Component	Subcomponent	Source	Cost (k$)	Responsible Institution
Beam line	Instrumentation			FNAL BD
Target		E866		FNAL PPD
M1	Coils	New	900	ANL
	Inserts	New	100	ANL
	Return Yoke	E866		FNAL PPD
	Assembly	New	220	FNAL PPD
	Power Supplies	E866		FNAL PPD
Jolly Green	Repair Coil			FNAL PPD
Giant	Assemble in Meson			FNAL PPD
	Power Supplies	E866		FNAL PPD
Station 1 MWPC	Chambers	E871 and E866		?, ACU, FNAL
	Electronics	E871 and E866		?, ACU, FNAL
	Readout	E871		?, ACU, FNAL
Station 1 Hodoscopes		New	20	ACU
Station 2 DC	Chambers	E866		Rutgers
	Electronics	E866		Rutgers
	Readout	New		FNAL PREP
Station 2 Hodoscopes		New	30	ACU
Station 3 DC	Chambers	E866		Rutgers
	Electronics	E866		Rutgers
	Readout	New		FNAL PREP
Station 3 Hodoscopes		New	30	ACU
Station 4 Prop. Tubes	Chambers	New	30	?, LANL
	Electronics	E866		LANL
	Readout	E871		LANL
Muon ID Wall	Assembly	E866		FNAL PPD
Gas System	Mixing	New		LANL
	Distribution	New		FNAL PPD
Station 4 Hodoscopes		New	80	ACU
Trigger		E866 and New	15	TAMU
	LRS2367	New	56	FNAL PREP
DAQ	Hardware	E871		?
	Software	E871 and New		?,VALPO,TAMU
Analysis	Software	E866		Lead - LANL

FNAL BD – Beams Division
FNAL PPD – Particle Physics Division
FNAL PREP – Physics Research Equipment Pool

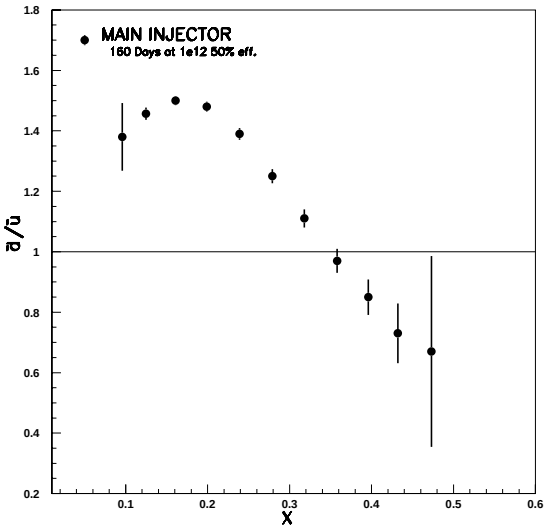

Figure 10: Projected results for the extraction of $\bar{d}/\bar{u}$ from a 160 day 50% efficiency run with 10^{12} protons per pulse on a 20" long liquid hydrogen and deuterium targets with the apparatus shown in Figures 7-8 based on the MRST [4] distribution of $\bar{d}/\bar{u}$.

approval of the proposal we will immediately request \$1.16M from DOE-NP for the construction of the magnet coils, inserts and the new hodoscopes. We anticipate the rest of the collaboration contributions coming from continuing research grants. Construction money for the coils could not become available before FY2000. We would estimate a 1 year coil construction and three month assembly process allowing for a tight installation schedule to achieve an early FY2002 start, consistent with the current ideas for the start of the Main Injector fixed target program.

4.1 Requests for FNAL

We specifically request FNAL to provide the following items:

- Repair coil of Jolly Green Giant Magnet
- Install Jolly Green Giant Magnet in Meson as a vertical bending magnet.
- Assemble M1 Magnet in Meson with the coil provided by ANL and return yoke from SM12.
- Provide beam dump with closed loop water recirculating cooling system.
- Provide Magnet Power Supplies.
- Provide Utilities (Power and Cooling Water) for Magnets and Power supplies.
- Move and install Muon ID absorber walls.
- Provide Beam line instrumentation

- Provide Liquid Hydrogen and Deuterium Targets and drive mechanism to interchange liquid and solid targets remotely.
- Prep Electronics. Essentially E866 Prep electronics plus 1700 channels of multi-hit TDC (LRS3377) , 16 LRS2367 units and 32 channels of mean-timers.
- Provide Chamber gas distribution system plumbing.
- Provide Flammable gas safety system.
- Provide Rigging for Installation
- Provide use of Lab 6 facilities for scintillator and light guide fabrication.
- Provide Counting House and Electronics areas with appropriate utilities installed.
- Two Analysis workstations for Counting House

5 Manpower

The core of the collaboration, Abilene Christian University, Argonne National Laboratory, Fermilab, Los Alamos National Laboratory, Texas A&M University and Valparaiso University has recently successfully completed the E866 Drell-Yan experiment at FNAL. These groups encompass the key technologies needed for the new measurements. The Rutgers group has experience in high rate drift chamber systems. Several other groups have expressed interest in the experiment and we expect little problem identifying sufficient manpower to construct, operate and analyze the experiment in a timely fashion following a favorable response from FNAL.

6 Summary

We propose to use the 120 GeV primary proton beam from the Main Injector to measure Drell-Yan yields for hydrogen, deuterium and three nuclear targets. These measurements will provide precise new information on:

- the ratio for $\bar{d}/\bar{u}$ and $\bar{d}-\bar{u}$ distributions of the proton over the x range of 0.2-0.45 and new insight into the non-perturbative origin of the parton distributions. (3.4 $\times$ 10^{18} incident protons).
- the nuclear dependence of the $\bar{u}$ distributions over a similar x range. (1.8 $\times$ 10^{18} incident protons).

The combination of these two measurements should also help resolve nuclear ambiguities inherent in obtaining nucleon antiquark distributions from neutrino data on nuclear targets. The total request for beam with 9 months of running at 10^{12} protons per pulse and 66% accelerator efficiency is 5.2 $\times$ 10^{18} protons.

References

[1] H. L. Lai *et al.*, Phys. Rev. D **55**, 1280 (1997).

[2] H. L. Lai *et al.*, hep-ph/9903282 (1999).

[3] A. D. Martin, R. G. Roberts and W. J. Stirling, Phys. Lett. B **419**, 1280 (1997).

[4] A. D. Martin, R. G. Roberts, W. J. Sterling and R. S. Thorne, Eur.Phys.J. **C4**, 463 (1998).

[5] P. Amaudruz *et al.*, Phys. Rev. Lett. **66**, 2712 (1991); M. Arneodo *et al.*, Phys. Rev. D **55**, R1 (1994).

[6] A. Baldit *et al.*, Phys. Lett. B **332**, 244 (1994).

[7] E866 Collaboration, E. A. Hawker *et al.*, Phys. Rev. Lett, **80** 3715 (1998).

[8] E866 Collaboration, J.-C. Peng *et al.*, Phys. Rev. D **58**, 092004 (1998).

[9] D. F. Geesaman, K. Saito and A. W. Thomas, Ann. Rev. Nucl. Part. Sci **45**, 337 (1995).

[10] A. D. Martin, W. J. Stirling and R. G. Roberts, Phys. Lett. B **252**, 653 (1990).

[11] D. A. Ross and C. T. Sachrajda, Nucl. Phys. B **149**, 497 (1979).

[12] W. Melnitchouk, J. Speth, and A.W. Thomas, Phys. Rev. D **59**, 014033 (1999).

[13] P. Geiger and N. Isgur, Phys. Rev. D **55**, 299 (1997).

[14] S. Kumano, Phys. Rev. D **43**, 3067 (1991); **43**, 59 (1991); S. Kumano and J. T. Londergan, Phys. Rev. D **44**, 717, (1991).

[15] A. Szczurek *et al.*, Nucl. Phys. A **596**, 397 (1996).

[16] G. t'Hooft, Phys. Rev. D **14**, 3432 (1976).

[17] A. E. Dorokhov and N. I. Kochelev, Phys. Lett. B **304**, 157 (1993).

[18] D. M. Alde *et al.*, Phys. Rev. Lett. **66**, 2285 (1991).

[19] F. Coester private communication; E. T. Berger, F. Coester and R. B. Wiringa, Phys. Rev. D **29**, 398 (1984).

[20] S. Gavin and J. Milana, Phys. Rev. Lett. **68**, 1834 (1992).

[21] S.J. Brodsky and P. Hoyer, Phys. Lett. B **298**, 165 (1993).

[22] R. Baier *et al.*, Nucl. Phys. B **484**, 265 (1997); R. Baier *et al.*, hep-ph/9804212.

[23] G. T. Bodwin, Phys. Rev. D **31**, 2616 (1985); **34**, 3932 (1986).

[24] G. T. Bodwin, S. J. Brodsky and G. P. Lepage, Phys. Rev. D **39**, 3287 (1989).

[25] V. Papavassiliou, Contribution to the Main Injector Stationary Target Workshop, Fermilab, May 1997.

[26] G. Moreno *et al.*, Phys. Rev. D **43**, 2815 (1991).

[27] C. A. Gagliardi *et al.*, Nucl. Instrum. Methods A **418**, 322 (1998).

[28] J. M. Jagger and K. M. Thompson, Cost estimate of P906 magnet.